The Use of a Railgun Facility for Dynamic Fracture of Brittle Materials

Markus Schneider, Gregory Vincent, James D. Hogan, and John G. Spray

***Abstract*— Linear electromagnetic acceleration has a wide range of applications. Among them are applications in the field of materials science, where relatively small, inexpensive systems can be of high value. For instance, it was shown recently at the French–German Institute of Saint Louis, France, that the symmetric Taylor test—a method to investigate the deformation behavior of specimens at high deformation rates—can be realized with higher precision than attainable with other acceleration methods using a railgun with velocity control. In this paper, we present another example for an application of a railgun in the field of materials science, namely, the study of impact phenomena and terminal ballistics. One of the major advantages of railgun technology is that the acceleration profile can be well defined at velocity ranges from very low speeds (<10 m/s) up to more than 2000 m/s—for one and the same launcher. Moreover, the geometry of a railgun projectile can be round, rectangular or, as in the case discussed here, hexagonal. Finally, electromagnetic acceleration does not require the use of propellants, which in the case of impact experiments could lead to complications—at least for the experimental application presented. The quest is to study the ejecta field of fractured brittle materials at moderate impact velocities (<500 m/s). It transpires that a railgun can be a valuable tool for such investigations. Using high-speed cameras and novel data processing methods ejecta distribution-velocity relations are explored. Our contribution describes the experimental setup used and will introduce some of the major results obtained so far.**

***Index Terms*— Electromagnetic launching, failure analysis.**

I. Introduction

WHILE research on railguns in the last decade has been mainly driven by military projects, it is worth pointing out the dual-use potential of this acceleration technology. Various suggestions have been made in the past ranging from railgun-assisted orbital launch of spacecraft to the injection of deuterium pellets into Tokamak fusion reactors [1]. At the ISL, we have recently pursued two projects in the field of materials science. The first project was related to the realization of a symmetric Taylor test [2]. It can be shown that railguns are very well suited to control the exit velocity and exit time by implementing a feedback circuit. Here, we report on an ongoing study in the field of impact physics. A research team from the University of New Brunswick (UNB) had the idea to investigate the fracture of brittle materials, such as natural and synthetic ceramics, at moderate impact velocities (v < 500 m/s). After discussion it transpired that ISL's SR3/60 hexagonal railgun would be an appropriate launcher to initiate the experimental study. The ensuing collaboration between UNB and ISL was characterized by an iterative approach. After each series of impact experiments the experimental setup and the diagnostic tools were improved, and the results reported to the impact physics community [3], [4]. In this publication, we report on the experimental setup used, the diagnostic tools that were developed and some illustrative results obtained. We also highlight the advantages of electromagnetic acceleration for these types of investigation for both the experiments performed and future projects. The latter are discussed with the help of corresponding simulations.

Manuscript received October 14, 2014; accepted January 21, 2015. Date of publication February 11, 2015; date of current version May 6, 2015.

M. Schneider and G. Vincent are with the French-German Research Institute, Saint Louis 68300, France (e-mail: markus.schneider@isl.eu; gregory.vincent@isl.eu).

J. D. Hogan is with the Hopkins Extreme Materials Institute, Johns Hopkins University, St. Baltimore, MD 21218 USA (e-mail: jd.hogan@jhu.edu).

J. G. Spray is with the University of New Brunswick, Fredericton, NB E3B 5A3, Canada (e-mail: jgs@unb.ca).

Color versions of one or more of the figures in this paper are available online at http://ieeexplore.ieee.org.

Digital Object Identifier 10.1109/TPS.2015.2396081

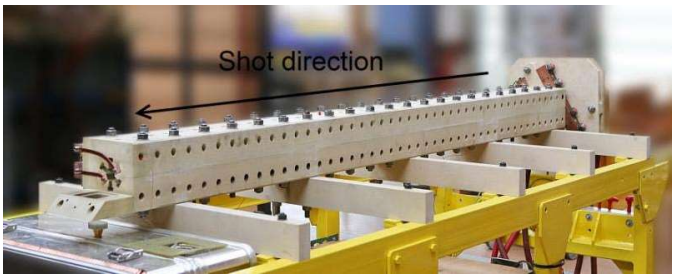

Fig. 1. Hexagonal segmented railgun SR3/60. Length of launch assembly: 2100 mm.

TABLE I
PARAMETERS OF SR3/60

Acceleration length	2100 mm
Electrical Energy per segment	Up to 2x 170kJ@10.5kV
Rail materials	CuCr1
Rail size	15x12 mm²
Hexagonal projectile calibre	28 mm
Inductance gradient	0.48 µH/m

II. Experimental Setup

A. Electromagnetic Accelerator

The ISL operates several small and medium caliber railguns. The hexagonal railgun SR3/60 is a facility used primarily to test and develop new concepts. The hexagonal geometry is reflected by three pairs of rails (segments) mounted at 120° to each other (Fig. 1). As a consequence, the projectile has a hexagonal cross section (see Fig. 3 below). Table I lists

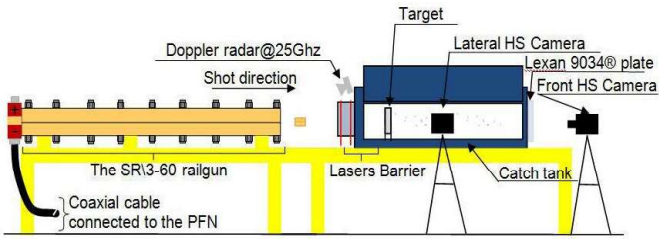

Fig. 2. Experimental setup.

the main parameters of the railgun. For further details on the launcher and its operational modes, we refer the reader to [5] and [6]. Here, we focus on the setup used for the impact experiments; a corresponding schematic is shown in Fig. 2. The railgun is equipped with a 25-GHz Doppler system to monitor the velocity during launch. In addition, laser barriers are installed to measure precisely and redundantly the impact velocity. The setup evolved during the series of experiments, especially with regard to camera use and positioning. The target is mounted inside a target holder, which itself is placed in the catch tank. This catch tank is suited for the observation of impacts because it allows for the monitoring of the event from the side (lateral camera) and from the front (front camera). For the experiments discussed here it was possible to work with a catch tank with open side windows. Only the front window was covered by a Lexan plate to protect the coaxial camera.

B. Ejecta Measurements Diagnostic Tool

A combined image enhancement and particle image velocimetry (PIV) algorithm implemented in MATLAB [7] was used to perform size and velocity measurements of fragments ejected from the rear of 7-mm-thick targets. A 62 g, 32-mm long aluminum projectile was used as the impactor at impact velocities ranging between 46 and 286 m/s (Mach 0.13–0.83; i.e., subsonic to transonic). Strain rates are estimated as the ratio of the target thickness to impact velocity and range between 6.50×10^3 and 4.09×10^4 1/s. The target material is an albite-rich granitoid (a natural rock of the granite family). A photograph of the target material and projectile is shown in Fig. 3(a). A Photron APX Ultima video camera filming at a frame rate of 8 kHz was used to record material ejected from the target. The size and velocities of fragments greater than 1 mm are recorded from high-speed camera images. An example of a high-speed video image is shown in Fig. 3(b). Note that the rear of the target is on the right of the image and the projectile is travelling from right to left. Initially, the x and y components of the velocity field are obtained using PIV. Positive x and y velocity follow the reference coordinates in Fig. 3(b). No assumption is made about the other component of the velocity in these calculations. In PIV, the velocity field is measured by recording the displacement of ejecta in gridded cells. Here, the region of interest is the rectangle in Fig. 3(b). All individual cells are not shown. Instead, an example is provided in the image. The velocity within a cell is calculated as follows: consider a particle in the ejecta field [Fig. 3(c)]; the particle at position x_t is tracked

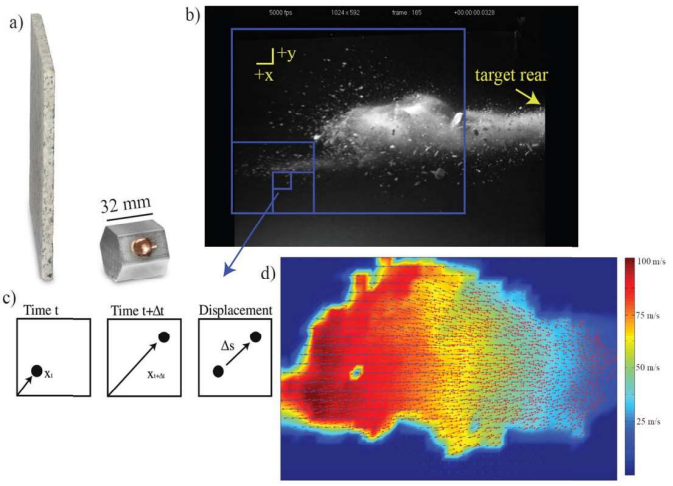

Fig. 3. (a) Photograph of 7-mm thick target with aluminum projectile. (b) High-speed video image of ejecta field with positive x and y directions labeled. The region of interest for the velocity measurements are also provided. (c) Concept of PIV, where individual cell velocities are obtained by tracking the displacement of a particle through time. (d) Contour of the gridded velocity field obtained using PIV (blue arrows) with projected fragment centroids (red arrows).

over two time intervals [left and center images in Fig. 3(c)]. The displacement, Δs, is then estimated (right image) and the cell velocity is obtained assuming velocity is equal to the ratio of displacement and time. Particle image velocity allows the velocity of all cells for all time to be computed. For additional information on PIV [8]. The next stage is to determine the spatial locations and sizes of ejecta. First, ejecta were made distinguishable using image enhancements implemented from the MATLAB image analysis toolbox [7]. The ejecta size, as it is referred to throughout this paper, is taken as the longest spanning dimension of the fragment in the high-speed video image frame. The minor axis dimension is taken perpendicular to the major axis. The volume of a fragment is obtained by multiplying the fragment area by an assumed thickness equal to the minor axis dimension. Centroids of individual ejecta are determined with the software and their locations are projected back onto the velocity field. Individual ejecta velocities are then obtained using a weighted average of their centroid distance from the adjacent cell center velocities. A contour of the gridded velocity field obtained using PIV (blue arrows) with projected fragment centroids (red arrows) is shown in Fig. 3(d).

III. Experimental Results

Experimental results for the combined size-velocity measurements are shown in Fig. 4. Initially, the cumulative distributions of mass larger than the corresponding ejecta size, L, is plotted in Fig. 4(a) for the highest and lowest strain rates under consideration in this investigation. This is not equivalent to a number-mass cumulative distribution. The distribution shifts to the left for an increase in strain rate from 6.57×10^3 to 4.08×10^4 1/s, indicating that fragments are decreasing in size for increasing strain rate. Also labeled in Fig. 4(a) for reference is the median value, $L_{50\%\text{mass}}$, in the mass-size representation of the information. $L_{50\%\text{mass}}$ is later plotted for all strain rates in Fig. 4(c). The cumulative distribution of mass greater than

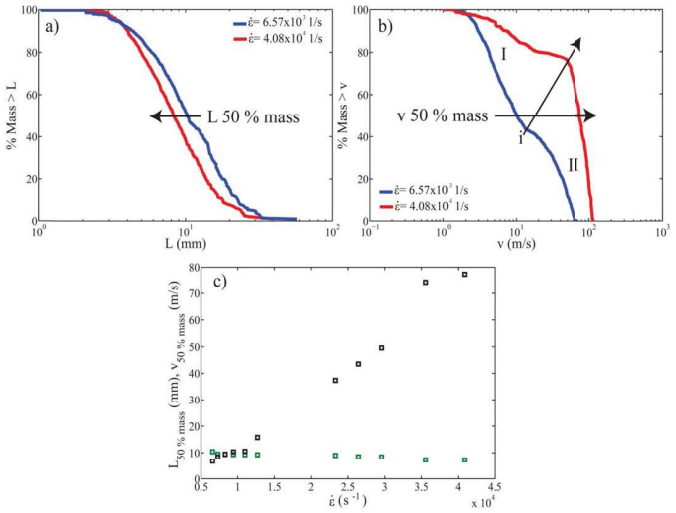

Fig. 4. (a) Cumulative distribution of mass greater than the corresponding size (millimeter). The median value in this representation is termed $L_{50\%\text{mass}}$ and is noted in the figure. (b) Cumulative distribution of mass greater than the corresponding velocity (meter/seconds). The median value in this representation is termed $v_{50\%\text{mass}}$ and is noted in the figure. (c) Values of $L_{50\%\text{mass}}$ and $v_{50\%\text{mass}}$ plotted against strain for a target thickness of 7 mm.

the corresponding velocity on the x-axis is shown in Fig. 4(b) for strain rates of 6.57×10^3 and 4.08×10^4 1/s. There are two distinct near-linear regions for both curves [labeled I and II in Fig. 4(b)]. Each region corresponds to a different material ejection mechanism, with region II being associated with a mechanism that expels material from the target rear more rapidly. The transition between two regions (labeled i near the lower strain rate curve) shifts upward and to the right, indicating that more material is being ejected at higher velocities when the strain rate is increased from 6.57×10^3 to 4.08×10^4 1/s. Also labeled in the figure is the median value, $v_{50\%\text{mass}}$, in the mass-velocity representation. The median values of the mass-size ($L_{50\%\text{mass}}$) and mass-velocity ($v_{50\%\text{mass}}$) cumulative distributions are plotted as a function of strain rate in Fig. 4(c). Note that the units on the y-axis are in millimeter for the ejecta size measurement and meter/seconds for ejecta velocity. Values of $L_{50\%\text{mass}}$ decrease slightly from 10.4 to 7.2 mm over this wide range in strain rate, indicating that the fragmentation mechanism is relatively insensitive to increasing strain rate. Values of $v_{50\%\text{mass}}$ increase for increasing strain rate, ranging from approximately 8–79 m/s. Values increase more rapidly at strain rates of 10^4 1/s. Combined, the distribution of mass among size and velocity can be used to validate numerical models and to better understand fragmentation and material ejection mechanisms during asteroid collision.

IV. Potential Future Impact Physics Experiments

The experiments performed have benefited from the use of electromagnetic acceleration in so far as this launch technique is precise, reproducible, and facilitates rapid relaunch (i.e., numerous experiments per day). The railgun design allows for a large range of precisely controlled velocities, a characteristic that had not been previously exploited by this laboratory.

TABLE II
Simulation Parameters and Results for Scenario 1

	Proj. 1	Proj. 2	Proj. 3
Projectile mass	62g	62g	62g
Charging Voltage	7.5 kV	7.5 kV	7.5 kV
Electrical Energy	2x87 kJ	2x87 kJ	2x 87 kJ
Delay betw. the 2 PFN	1 ms	1 ms	1 ms
Velocity	153 m/s	153 m/s	153 m/s
Impact Time	20.7 ms	25.7 ms	28.2 ms
Kinetic Energy	725 J	725 J	725 J
t_{impact} - t_{fire}	20.7 ms	20.7 ms	20.7 ms

In this following section we highlight another advantage of the railgun, namely its potential to be used as a multishot system. The ISL has developed multishot railgun technology allowing for both high fire rates and muzzle speeds [9]. The SR3/60 can also be operated in multishot mode, as it has three independent pairs of rails [10]. As has been argued in the past with respect to operational scenarios, electromagnetic multishot railguns are able to fire intelligent salvos [11]. An electromagnetic system allows for varying both the muzzle velocity of the projectile and the fire rate during a burst. In contrast, classical multishot guns are operated at constant fire rate and muzzle speed. While it is clear that this capability translates into a considerable strategic advantage for future electromagnetic weapon systems [10], we focus here on its potential in the field of impact physics. This is done by carrying out simulations for four different impact scenarios. For our purpose, it is sufficient to solve the Kirchhoff equations describing the electric circuit, and to couple them with the dynamics of the projectile using Newton's second law. This can be done conveniently using a SPICE code, see for instance [11]. The PSPICE model used for simulating the SR3/60 resembles that presented in [11], and therefore allows for calculating the dynamics of the projectile. Note that the model used here does not include physical effects, such as the velocity skin effect or friction, which would in many cases have to be considered for matching experimental results. We felt that for the purpose of illustrating the capacity of multishot technology the approach taken here is appropriate. The first scenario deals with the impact of three projectiles with the same speed and mass but a varying fire rate to illustrate one of the basic advantages of electromagnetic railguns. The corresponding simulation parameters and results are shown in Table II and in Fig. 5, respectively. This sequence is realized using the same charging voltage for all three shots. As the delay between the two capacitor banks is also kept constant, the resulting current pulses and projectile velocities are equal for all three shots. Only the trigger times are varied in such a manner that within the burst of three shots the fire rate is not constant. Fig. 5 shows the current profiles, as well as the projectile dynamics for all the three shots. The current amplitudes reach 200 kA and the velocity is 153 m/s. As is expected, the trigger times define the sequence of impacts. The projectiles reach the target at 20.7, 25.7, and 28.2 ms, respectively, realizing the case of

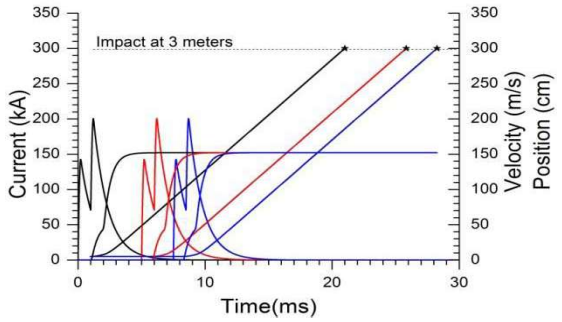

Fig. 5. Current profiles and projectile dynamics of scenario 1.

TABLE III
SIMULATION PARAMETERS AND RESULTS FOR SCENARIO 2

	Proj. 1	Proj. 2	Proj. 3
Projectile mass	62g	62g	49.6g
Charging Voltage	7.5 Kv	7.5 kV	7.5 kV
Electrical Energy	2x 87 kJ	2x 87 kJ	2x 87 kJ
Delay betw. the 2 PFN	1 ms	1 ms	2 ms
Velocity	153 m/s	153 m/s	156 m/s
Impact Time	20.7 ms	25.7 ms	28.2 ms
Kinetic Energy	725 J	725 J	603 J
t_{impact} - t_{fire}	20.7 ms	20.7 ms	20.7 ms

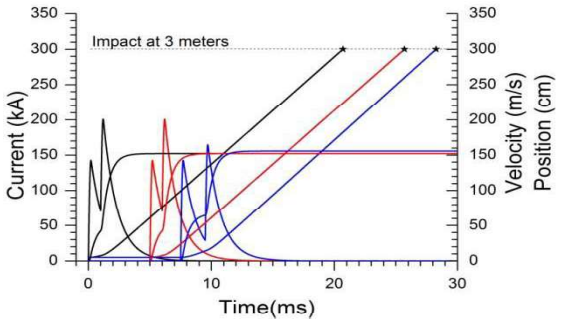

Fig. 6. Current profiles and projectile dynamics of scenario 2.

TABLE IV
SIMULATION PARAMETERS AND RESULTS FOR SCENARIO 3

	Proj. 1	Proj. 2	Proj. 3
Projectile mass	62g	62g	62g
Charging Voltage	7.5 Kv	8.5 kV	10 kV
Electrical Energy	2x87 kJ	2x112 kJ	2x 155kJ
Delay betw. the 2 PFN	1 ms	0.856 ms	0.603 ms
Velocity	153 m/s	204 m/s	306 m/s
Impact Time	20.7 ms	20.7 ms	20.7 ms
Kinetic Energy	725 J	1290 J	2902 J
t_{impact} - t_{fire}	20.7 ms	15.7 ms	10.7 ms

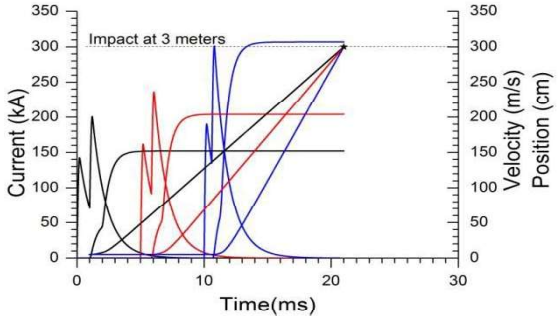

Fig. 7. Current profiles and projectile dynamics of scenario 3.

TABLE V
SIMULATION PARAMETERS AND RESULTS FOR SCENARIO 4

	Proj. 1	Proj. 2	Proj. 3
Projectile mass	62g	30g	14g
Charging Voltage	7.5 Kv	7.3 kV	5.4 kV
Electrical Energy	2x87 kJ	2x82 kJ	2x 45 kJ
Delay betw. the 2 PFN	1 ms	3.06 ms	1.35 ms
Velocity	153 m/s	219 m/s	321 m/s
Impact Time	20.7 ms	25.7 ms	28.2 ms
Kinetic Energy	725 J	720 J	721 J
t_{impact} - t_{fire}	20.7 ms	15.7 ms	10.7 ms

a nonconstant fire rate. However, all projectiles have the same kinetic energy. In scenario 2, we consider an impact sequence where we realize the same impact times as in scenario 1, but we change the kinetic energy of the last projectile of the sequence. The corresponding simulation parameters are given in Table III. As can be seen, to obtain the desired impact sequence we had to change both the mass of the current pulse for the third projectile. The kinetic energy of the third projectile is 603 kJ being lower than that for the two others. Fig. 6 shows the corresponding projectiles dynamics. Having shown the capacity of the electromagnetic system using typical scenarios, we will now look at a hypothetical case. We consider the case of realizing an impact of three projectiles at the same point and at the same time. To obtain such an impact we have of course to vary the velocity of the different projectiles. The parameters required for one possible solution of the impact scenario are shown in Table IV. As can be seen, we are using the same mass, and therefore the kinetic energies of the projectiles vary. In Fig. 7, the projectile dynamics and the current profiles are drawn. Note that realizing this impact sequence is not a straightforward process, as can be seen from the varying parameters in Table IV, or the varying current pulses in Fig. 7, respectively. Our final scenario 4 considers basically scenario 3 and adds an additional condition: the projectiles should arrive at the same time at the same point with the same kinetic energy.

The corresponding parameters are given in Table V and the simulation results can be found in Fig. 8. As can be seen, it is possible to find solutions. However, in comparison with Table IV, the last remaining constant parameter, the mass of the projectiles, had to be varied. We conclude our considerations at this point with the remark that it we do of course not think that it is surprising that solutions for our scenarios exist. However, we felt that giving some examples is appropriate to hopefully

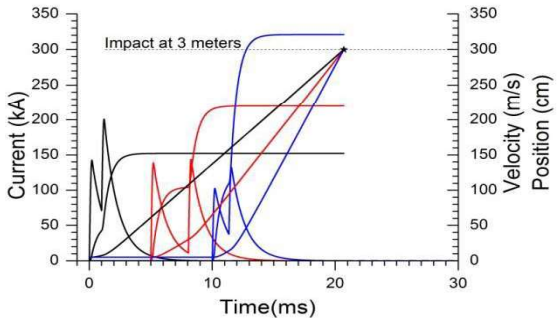

Fig. 8. Current profiles and projectile dynamics of scenario 4.

catch the attention of possible users of such a versatile tool for impact experiments and to stimulate their imagination.

V. Conclusion

Techniques and methodologies presented here have been successfully implemented to study fragmentation and material ejection mechanisms during impact into planetary materials. The applicability of ejecta tracking techniques and methodology, in conjunction with the electromagnetic launch technology, can be used to improve current impact testing and provide critical details and validation for numerical codes. The advantages of electromagnetic acceleration for these kinds of investigations have been highlighted by discussing selected impact scenarios, which could be of interest to scientists working in this field. In particular, the case of sequential impacts has been considered.

References

[1] R. A. Marshall and W. Ying, *Railguns: Their Science and Technology*. Beijing, China: China Machine Press, 2004.

[2] T. Siaenen, M. Schneider, P. Zacharias, and M. J. Loeffler, "Actively controlling the muzzle velocity of a railgun," *IEEE Trans. Plasma Sci.*, vol. 41, no. 5, pp. 1514–1519, May 2013.

[3] J. D. Hogan, J. G. Spray, R. J. Rogers, G. Vincent, and M. Schneider, "Dynamic fragmentation of planetary materials: Ejecta length quantification and semi-analytical modelling," *Int. J. Impact Eng.*, vol. 62, pp. 219–228, Dec. 2013.

[4] J. D. Hogan, J. G. Spray, R. J. Rogers, G. Vincent, and M. Schneider, "Dynamic fragmentation of planetary materials: Sub-hypervelocity ejecta measurements and velocity scaling," *Planet. Space Sci.*, vol. 87, pp. 66–77, Oct. 2013.

[5] S. Hundertmark and G. Vincent, "Performance of a hexagonal, segmented railgun," in *Proc. IET Eur. Pulsed Power Conf.*, Sep. 2009, pp. 1–4.

[6] S. Hundertmark, "Comparing a dynamic railgun simulation with experiment," *J. Elect. Eng.*, vol. 11, no. 4, 2011, Art. ID 11.4.6.

[7] *MATLAB User Manual*, Mathworks, Natick, MA, USA, 2013.

[8] R. J. Adrian and J. Westerweel, *Particle Image Velocimetry*, vol. 30. Cambridge, U.K.: Cambridge Univ. Press, 2010.

[9] M. Schneider, M. Woetzel, W. Wenning, and D. Walch, "The ISL rapid fire railgun project RAFIRA part I: Technical aspects and design considerations," *IEEE Trans. Magn.*, vol. 45, no. 1, pp. 442–447, Jan. 2009.

[10] G. Vincent and S. Hundertmark, "Using the hexagonal segmented railgun in multishot mode with three projectiles," *IEEE Trans. Plasma Sci.*, vol. 41, no. 5, pp. 1431–1435, May 2013.

[11] J. Gallant, T. Vancaeyzeele, B. Lauwens, B. Wild, F. Alouahabi, and M. Schneider, "Design considerations for an electromagnetic railgun firing intelligent bursts to be used against anti-ship missiles," in *Proc. 17th Int. Symp. EML*, San Diego, CA, USA, Jul. 2014, pp. 1–6.

[12] J. Wey, E. Spahn, and M. Lichtenberger, "Railgun modeling with the P-Spice code," *IEEE Trans. Magn.*, vol. 33, no. 1, pp. 619–625, Jan. 1997.

Authors' photographs and biographies not available at the time of publication.